Magnetic anisotropy and Verwey transition of magnetosome chains in *Magnetospirillum gryphiswaldense*

Andreas U. Gehring,[1] Håkon Fischer,[1] Michalis Charilaou[1] and Inés García-Rubio[2]

[1]*Institute of Geophysics, ETH Zurich, 8092 Zurich, Switzerland. E-mail: agehring@ethz.ch*
[2]*Laboratory of Physical Chemistry, ETH Zurich, 8093 Zurich, Switzerland*

SUMMARY

Magnetotactic bacteria (MTB) are characterized by cellular magnetic dipoles formed by the 1-D assembly of magnetite and/or greigite particles aligned along their magnetic easy axes. This alignment creates strong interaction-induced shape anisotropy. Ferromagnetic resonance (FMR) spectroscopy is applied to study the changes in anisotropy of the MTB *Magnetospirillum gryphiswaldense* between room temperature and 10 K. The Verwey transition is found at about 100 K. The characteristic FMR signal of the cellular dipole at room temperature vanishes upon cooling to the isotropic point at $T_i \approx 130$ K, where the magnetocrystalline anisotropy constant K_1 becomes zero. Monitoring of the FMR response of intact MTB as a function of temperature is taken to discuss theoretically the reduction of the interaction-induced shape anisotropy in magnetofossils because of diagenetic processes. It is concluded that there is a similarity in the FMR response between magnetofossils at room temperature and intact MTB near T_i. This is because the critical effect of the magnetocrystalline anisotropy constant K_1 and of the alignment of magnetic easy axes on the cellular dipole. Low-temperature FMR results of intact MTB can thus be used as a guideline for detecting magnetofossils in geological environments.

Key words: Biogenic magnetic minerals; Environmental magnetism; Magnetic fabrics and anisotropy.

1 INTRODUCTION

The anisotropy of magnetite chains in bacterial cells have long been of considerable interest because they can provide an insight into the functionality of magnetotactic bacteria (MTB) and can be used for their identification in geological samples (Mann *et al.* 1987; Dunin-Borkowski *et al.* 1998; Frankel 2003; Weiss *et al.* 2004; Kopp & Kirschvink 2008; Faivre *et al.* 2010;). Many magnetic and microscopic laboratory studies on intact MTB have shown that the assembly of magnetite chains generates a cellular magnetic dipole, which is utilized as a compass that allows the bacteria to navigate along the Earth's magnetic field toward their favourable habitats (Bazylinski & Frankel 2004). This kind of utilization of the Earth's magnetic field is referred to as magnetotaxis. The detection of fossil MTB in geological systems is ambiguous, because diagenesis leads to the decay of the cellular matter and the disintegration or collapse of the magnetite chains. Such magnetofossils, however, are the critical pre-condition for unravelling the evolution of magnetite biomineralization and magnetotaxis in Earth's history (Kopp & Kirschvink 2008). Moreover, because MTB typically live in the oxic–anoxic transition zones of aquatic environments, magnetofossils can be taken as a redox indicator and can be used as a constraint for the reconstruction of palaeoclimates (Simmons *et al.* 2006; Paasche & Larson 2010).

In intact MTB, well-crystallized magnetite particles are usually enveloped by biomembranes, termed magnetosomes. They generally exhibit a narrow grain size distribution within a magnetically stable single domain (SSD) range. The membrane-bound magnetite particles are generally aligned with a [111] crystallographic axis parallel to the magnetosome chain axis and the gap sizes between adjacent magnetosomes are small (Mann *et al.* 1984; Pósfai *et al.* 2006). This chain configuration is prevented from magnetostatic collapse by intracellular cytoskeletal filaments (Scheffel *et al.* 2006) and it increases the total dipole moment of the assembly, which can be considered as the algebraic sum of the moments of the individual magnetosomes (Frankel *et al.* 1979). Such an assembly creates interaction-induced shape anisotropy (Jacobs & Beans 1955; Penninga *et al.* 1995; Hanzlik 2002).

The characteristic properties of bacterial magnetite, that is, grain size distribution and chain assembly, have been analysed extensively by transmission electron microscopy (TEM; Petersen *et al.* 1986; Devouard *et al.* 1998; Dunin-Borkowski *et al.* 1998). Apart from microscopy, magnetic methods have been applied to detect intact MTB and their fossil remains in sediments (e.g. Snowball 1994; Li *et al.* 2009; Egli *et al.* 2010). Among these methods, analyses of remanent magnetization and coercivity have been used, which mainly provide information about the domain state of magnetite and indirectly about the grain size. Ferromagnetic resonance (FMR)

GJI Geomagnetism, rock magnetism and palaeomagnetism

spectroscopy has been applied successfully to study MTB and their mineral remains by providing, in addition to evidence of the domain state, direct information about the magnetic anisotropy resulting from the assembly of magnetosomes in chains (Weiss *et al.* 2004; Fischer *et al.* 2008; Kopp & Kirschvink 2008; Mastrogiaccomo *et al.* 2010; Gehring *et al.* 2011). In a recent paper, Charilaou *et al.* (2011) presented an approach to simulate FMR spectra obtained from MTB based on physical principles.

A specific test for the presence of MTB and magnetosomes—also known as the Moskowitz test (Moskowitz *et al.* 1993)—is based on the magnetic response of chains of SSD magnetite at the Verwey transition (T_V). At this intrinsic transition, magnetite undergoes a structural change from cubic to monoclinic, which results in a prominent change in the magnetization properties (e.g. Verwey 1939; Muxworthy & McClelland 2000; Walz 2002; Wright *et al.* 2002; Gracia & Subias 2004). Above T_V, an additional transition occurs, the isotropic point (T_i) at which the first-order fourfold anisotropy constant K_1 of magnetite becomes zero (Bickford 1950). For pure magnetite, T_V is found at about 125 K and T_i at a slightly higher temperature of about 130 K (e.g. Bickford 1950; Özdemir *et al.* 2002; Walz 2002). Above T_i with $K_1 < 0$, the crystallographic [111] directions in magnetite are the magnetic easy axes whereas the [100] directions are the hard axes. Below T_i but above T_V, $K_1 > 0$, the magnetic easy axis shifts from the [111] to the [100] direction, which diminishes the interaction-induced shape anisotropy. The goal of this study is to analyse changes of the cellular magnetic dipoles in intact MTB as function of temperature by means of FMR spectroscopy. The spectral changes are discussed in the context of the decrease of interaction-induced shape anisotropy as it can occur for magnetofossils in geological systems.

2 SAMPLE AND METHODS

A freeze-dried sample of cultured MTB *Magnetospirillum gryphiswaldense* strain MSR-1 was used. The preparation of *M. gryphiswaldense* followed the protocol of Heyden & Schüler (2003) and is further described in the paper by Fischer *et al.* (2008). To protect the magnetosomes from oxidation the sample was sealed in paraffin for the magnetic measurements. Before the magnetic and FMR spectroscopic analyses the presence of magnetosome chains was checked by TEM. Details of the MTB preparation and the TEM results are described by Fischer *et al.* (2008). The temperature dependence of the magnetization was measured in a Quantum Design physical property measurement system, by zero-field cooling (ZFC) and field cooling (FC) cycles using a weak field of 5 mT, which is insufficient to saturate the sample but large enough to magnetize the magnetosomes and to detect the T_V. In this procedure, the magnetizations were measured upon heating the sample between 10 and 300 K in a 5 mT field after first cooling in zero field and then in a 5 mT field.

FMR spectroscopy was performed to analyse the anisotropic properties of the MTB. In a FMR experiment, the precessional motion (Larmor precession) of the magnetization in an external magnetic field is sustained by a microwave magnetic field, perpendicular to the external field. In a field-sweep experiment, resonance occurs when the Larmor frequency of the magnetic moments coincides with the microwave frequency. The resonance equation can be written as $h\nu = g\,\mu_B\,B$, where h is Planck's constant, ν is the microwave frequency, μ_B the Bohr magneton (9.274×10^{-24} Am^2), g the gyromagnetic factor and B is the applied dc magnetic field. The external field adds to the internal magnetic field B_{int}, which

cannot be measured directly. In the resonance equation the g takes into account the effect of B_{int}, which contains different contributions, such as the demagnetization field (shape anisotropy), the magnetocrystalline anisotropy and magnetostrictive energies. The last contribution can be neglected because of the submicron size of the particles.

Because the magnetite chains of the MTB are oriented randomly in the bulk sample, and each chain orientation fulfils a specific resonance condition, the measured net signal is the superposition of all resonance events, that is, the measured spectrum is the sum of the spectra originated from particles in all orientations. For this spectrum we define B_{res} as the applied magnetic field at maximum absorption, which means the zero crossing in the derivative spectrum. The corresponding splitting factor defined as g_{eff} can be extracted using the resonance equation. The parameter ΔB_{eff} considered as the effective line-width, is derived from the absorption spectrum and is described as the full width at half the maximum (FWHM) amplitude of the absorption (e.g. Weiss *et al.* 2004; Faivre *et al.* 2010). The line-width for a particular orientation is a result of magnetic damping. The dominant mechanism is Gilbert damping, which is caused by a combined effect of exchange interaction and spin–orbit coupling (magnetocrystalline anisotropy) and can be thought of as viscous force acting on the magnetization vector during the precession. The temperature dependences of the strength of the spin–orbit coupling and the exchange interactions are similar to those of the magnetocrystalline anisotropy and the magnetization, respectively (Heider & Williams 1988; Özdemir *et al.* 2002). The apparent line-width of the signal obtained from the MTB bulk sample, however, is the sum of resonances from all anisotropic contributions of magnetosome chains oriented at random angles (Charilaou *et al.* 2011). Therefore, the effective line-width ΔB_{eff} is the result of this superposition of signals, and is thus a direct index of the difference between the easy axis and hard axis of magnetization.

For the FMR measurement the sample was fixed with paraffin in a standard ESR glass tube with a diameter of 4 mm. The spectra were recorded on a Bruker E500 spectrometer working at X-band (microwave frequency 9.47 GHz). The temperature of the sample in the cavity was controlled by means of a helium gas-flow cryostat ESR 910 (Oxford Instruments) which allowed performing measurements from 10 K to room temperature. A modulation amplitude of 1 mT and microwave power of 0.063 mW were used for the measurements. The ZFC/FC experiments were performed at 10 K first by cooling the sample in the cavity from room temperature in the absence of a magnetic field and followed by warming up the sample to RT and cooling again to 10 K in a 0.8 T field. The low-temperature series was performed after cooling the sample in the spectrometer cavity to 10 K while the magnet was switched off. The measurements were conducted in two cycles on the same sample and the data showed a high reproducibility. In addition to the FMR measurements, the spectra obtained at room temperature and 130 K were simulated using the model by Charilaou *et al.* (2011).

3 RESULTS AND DISCUSSION

3.1 Static magnetization of magnetosomes

The sample check under the TEM showed magnetite particles of about 50 nm with nearly equidimensional morphology, assembled in chains. The size and the morphology of the magnetosomes are typical for *M. gryphiswaldense* strain MSR-1 (Scheffel *et al.* 2006; Ding *et al.* 2010). The ZFC/FC measurements of the MTB sample
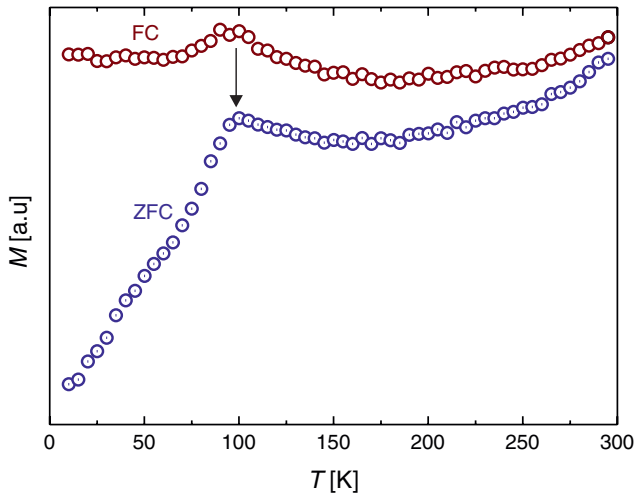
Figure 1. Variation with temperature of the magnetization of the MTB sample under ZFC and FC conditions; the temperature of the Verwey transition is arrowed.

Figure 2. (a) FMR spectra at room temperature before (solid line) and after cooling (dashed line); (b) spectra at 10 K after cooling in a zero field (solid line) and cooling in a 0.8 T field (dashed line). The vertical line corresponds to $g = 2$.

show that compared to FC, the ZFC curve exhibits a pronounced increase upon heating to 100 K (Fig. 1). Above this temperature the ZFC and FC curves are similar. The change in the behaviour at 100 K is indicative of the T_V (Prozorov *et al.* 2007). The difference between ZFC and FC measurements below T_V arises from the increase in magnetocrystalline anisotropy below T_V (Özdemir *et al.* 2002). Compared to pure synthetic magnetite with $T_V \approx 120$ K, the magnetosomes exhibit a slightly lower transition temperature, which is probably because of minor oxidation (Kakol & Honig 1989; Pan *et al.* 2005; Prozorov *et al.* 2007).

3.2 Room temperature versus 10 K FMR spectra

In this paragraph the FMR spectral response at temperatures far above and below T_V are presented to test the effect of the T_V on the MTB sample. The spectrum at room temperature ($T = 290$ K) exhibits an asymmetric line-shape, in which the extended low-field absorption has two distinct positive features, a line-width $\Delta B_{\text{eff}} = 126.4$ mT and a resonance field $B_{\text{res}} = 369.2$ mT corresponding to $g_{\text{eff}} = 1.83$ (Fig. 2). The spectral parameters indicate mature *M. gryphiswaldense* as previously reported by Fischer *et al.* (2008). The $g_{\text{eff}} < 2$ suggests that interaction between SSD magnetite particles stabilized in membranes along cytoskeletal filaments cause cellular magnetic dipoles (Weiss *et al.* 2004). Each dipole creates a predominantly demagnetizing internal field that is in the opposite direction to the external field, that is, it generally increases B_{res} that applies mostly to the perpendicular orientation. The spectrum indicates anisotropy dominated by uniaxiality and the two low-field resonance peaks can be interpreted as an effect because of chains aligned parallel and perpendicular to the external field (Kopp *et al.* 2006; Fischer *et al.* 2008; Faivre *et al.* 2010). The parallel alignment causes resonance at lower field compared to the perpendicular alignment. The shoulder close to B_{res} could be generated by cubic anisotropy contribution (Charilaou *et al.* 2011). The spectroscopic properties, however, clearly suggests that the linear assembly of the magnetosomes effectively removes the degeneracy among the three [111] easy axes and it distinguishes the one easy axis along the chain axis, that is, the easy magnetization axis of the magnetosomes in *M. gryphiswaldense* are aligned. Electron holography of different
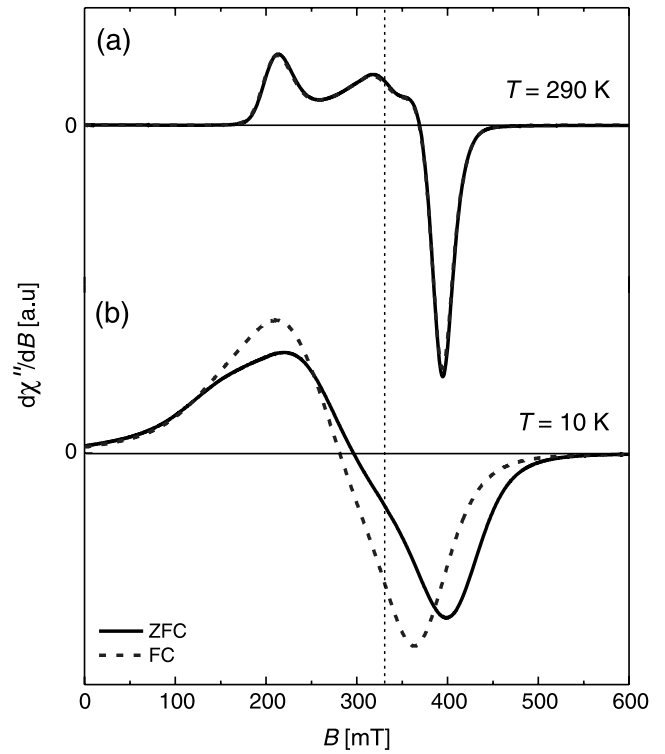
strains of *Magnetospirillum* at room temperature shows stray fields with highly parallel and straight lines following the magnetosome chains (Dunin-Borkowski *et al.* 1998; Simpson *et al.* 2005) and agrees well with this interpretation.

The spectrum at 10 K after ZFC was different from that at 290 K (Fig. 2). The low-temperature spectrum was less asymmetric and no distinct low-field resonance features were found. This is because of the symmetry change of magnetite at T_V and the subsequent departure from preferential spin alignment along the chain axis. Such a change yields diffuse anisotropic contributions with indistinct resonance regimes, which are indicated by the asymmetry and smearing out of the line-shape. B_{res} shifts to a lower value of 296.3 mT because below T_V the magnetocrystalline anisotropy increases prominently and becomes dominant over shape anisotropy. This change of anisotropic behaviour accompanies the broadening of $\Delta B_{\text{eff}} = 205.3$ mT at 10 K, which is indicative of an increase of the total anisotropy field.

To estimate the effect of spin alignment along the chains, we repeated the experiment, but this time under FC of the sample in a field $B = 0.8$ T which saturates the sample. This yielded $g_{\text{eff}} = 2.41$, that is, $B_{\text{res}} = 280.5$ mT and a narrowing of the spectrum to $\Delta B_{\text{eff}} = 173.1$ mT. The spectral changes are the result of structural and magnetic modifications at T_i. As mentioned above, the easy axes of the magnetosomes are nearly aligned parallel to the chain axes of MTB at room temperature. At T_V, the easy axes are switched from the [111] to the [100] direction. Numerical study by Muxworthy & Williams (2006) suggests that under ZFC condition interacting magnetosomes select one of the [100] directions on passing through T_V, whereby the history of the magnetic moment biases the selection. By contrast, under FC conditions, the [100] direction, which is closest to the applied field direction becomes

the new easy axis along which the spins are pinned. Such induced preferential alignment creates a higher induced remanence under FC than under ZFC conditions (Moskowitz *et al.* 1993). During the FMR experiment the magnetic induction in the ZFC sample begins from a quasi-demagnetized state and a wide range of internal static fields are generated by the sweeping field. Because the induction of the FC samples starts from a remanence state, the variation of the internal field occurs in a narrower range. Thus the reduction ΔB_{eff} by about 15 per cent in the FC sample compared to the ZFC one is likely to be caused by the increase in magnetization, which also can explain the shift of B_{res} for the FC compared to the ZFC sample.

3.3 Spectral changes between 10 K and room temperature

As seen above, cooling through T_V erases the alignment of the easy axes along the magnetosomes chains. In the following, we investigate the generation of the easy axes alignment in magnetite chains with temperature. The spectrum at 10 K revealed a broad low-field resonance with no distinguishable peaks (Figs 2b and 3). Above T_i, at about 140 K, the first indication of the development of two distinct low-field features was observed and at higher temperature the shoulder became more pronounced and at about 180 K two distinct features were detectable. Simultaneously, the high-field shoulder associated with the perpendicular component appeared. The two features and this shoulder became more pronounced with increasing temperature and reach a maximum at about 260 K (Fig. 3). At the same time the asymmetry of the signal enhanced. The spectra before and after the low-temperature measurements are identical, which suggest that the effect of T_V is reversible (Fig. 2a).

Upon warming the spectral parameter B_{res} revealed a decrease between 10 and 30 K and increased between 40 and 290 K. The corresponding g_{eff} values exhibited a maximum between 30 K and 40 K followed by a steady decrease to $g_{eff} = 1.83$ at room temperature (Fig. 4). FMR absorption of single crystal magnetite with the applied field aligned along the easy axis of magnetization showed a different behaviour of the g value with temperature compared to the magnetosome chains; at room temperature $g_{eff} = 2.12$ and a monotone decrease with decreasing temperature was found (Bickford 1950). The difference of the g_{eff} values of the single crystal and magnetite chains is most pronounced at room temperature (Fig. 4). The lower g_{eff} value of the magnetite chains indicates a relatively higher B_{res}, which can be explained by the pronounced shape anisotropy dominated by the contribution of the perpendicular component. At lower temperatures, the difference of g_{eff} values of the MTB compared to the single crystal diminished and at 130 K their g_{eff} values become the same. For magnetite, this temperature is equivalent to the isotropic point T_i where $K_1 = 0$, that is the easy axes are randomly distributed (Bickford 1950). Considering the magnetosome chains, $K_1 = 0$ means that the contribution of the alignment of easy axes to the overall anisotropy is lost. To support this argument, the spectra at room temperature and T_i were simulated with the model by Charilaou *et al.* (2011) (Fig. 5). At room temperature the spectrum can be fitted using $B_{uni} = 96$ mT and $B_{cub} = 22$ mT, which corresponds to the K_1 of magnetite. The spectrum at T_i can be simulated with $B_{uni} = 78$ mT, under the assumption that $B_{cub} = 0$. The decrease of B_{uni} by 18 mT is because of the reduced projection of the magnetization along the chain and clearly indicates the effect of easy-axis shifting upon approaching the T_V. In addition, the fitting of the spectrum at T_i requires broader signals for the resonance components, and, therefore, the low-field
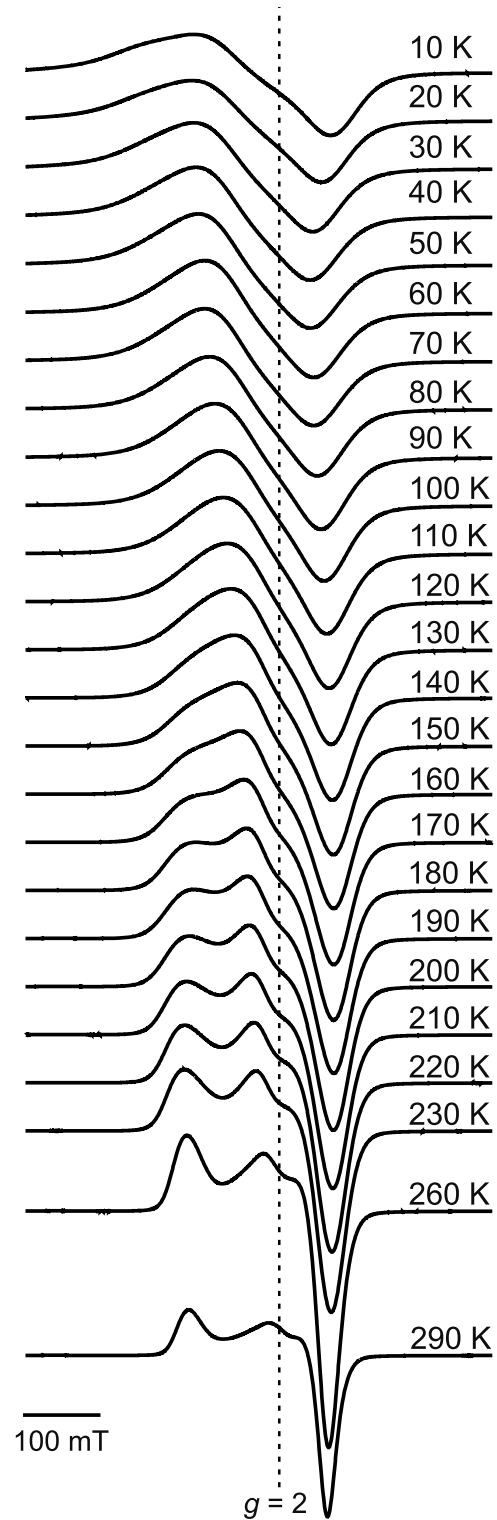

Figure 3. Series of FMR spectra of the MTB sample upon warming.

features found at room temperature are smeared out at T_i. Moreover, the high-field shoulder indicative of perpendicular alignment of the chains to the external field is also absent at T_i (Fig. 3). In general, the FMR line-width is caused by anisotropy and damping mechanisms, whereas the latter is among others influenced by structure, finite size effects and electrical conductivity. In the context of anisotropy-induced line broadening, however, the observed change of ΔB_{eff} is
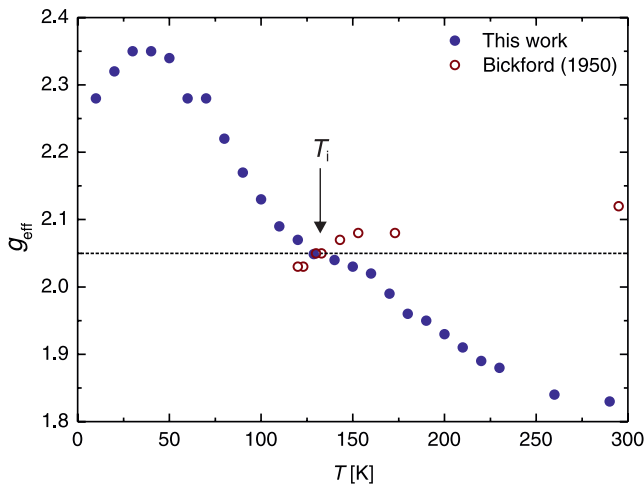
Figure 4. The g_{eff} values of the MTB sample upon warming (dots) and published g values for single crystal magnetite (circles); the isotropic point T_i is arrowed.
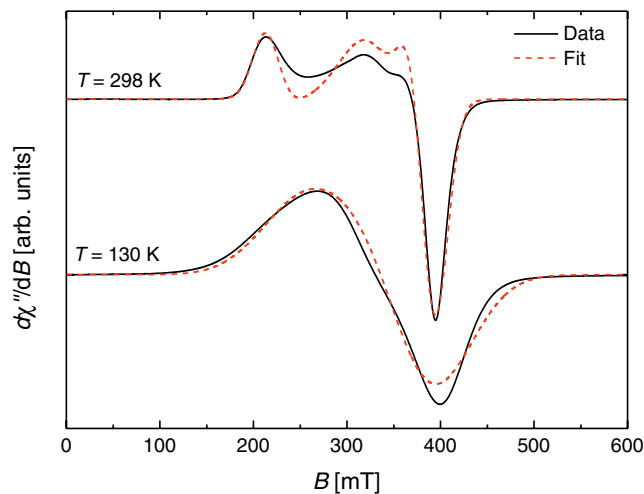

Figure 5. Recorded (solid lines) and simulated (dashed lines) FMR spectra of MTB at $T = 298$ and 130 K. For $T = 298$ K, the simulation parameters for the anisotropy are $B_{uni} = 96$ mT and $B_{cub} = 22$ mT, whereas for $T = 130$ K they are $B_{uni} = 78$ mT and $B_{cub} = 0$. The simulated signals are superpositions of Gaussian profiles of each orientation with a fixed line-width, which was found to be 25 mT for 298 K and 45 mT for 130 K, respectively.

due to the increase in the total anisotropy in the magnetite nanoparticles close to T_v (Fig. 6). Above T_i, the two distinctive peaks and the shoulder grow continuously and are well developed at about 200 K. Because the magnetocrystalline anisotropy of aligned magnetosomes influences the shape anisotropy of the chain, the development of the uniaxial features with temperature is affected by $|K_1|$ (Fischer *et al.* 2008). The simultaneous increase in B_{res} is in good agreement with the strengthening of the cellular magnetic dipoles in MTB. Considering the ZFC–FC magnetization curves, the relative steep increase in g_{eff} at about 100 K can be assigned to the T_V (Figs 1 and 4). Moreover, the transition at lower temperature indicated by g_{eff} below 50 K is probably because of the cease of electron hopping in the magnetite lattice (Kronmüller & Walz 1980; Fischer *et al.* 2008). In this context, electron hopping corresponds to fluctuation of the electron density, which in turn, influences the spectroscopic splitting factor.
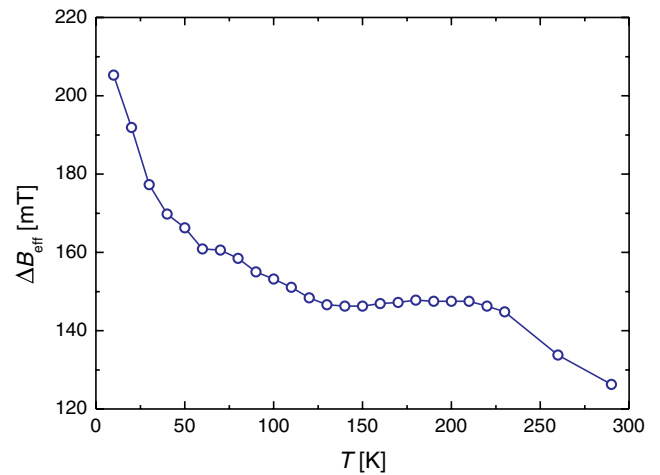
Figure 6. The change of the effective line-width, ΔB_{eff}, upon warming.

The line-width, ΔB_{eff}, generally decreased with increasing temperature (Fig. 6). The most pronounced narrowing was found below T_V. Above T_i, ΔB_{eff} varied little up to 230 K and between this temperature and 290 K a distinct decrease was found. This behaviour of ΔB_{eff} upon warming indicates a lowering of the overall anisotropy in the system. The decrease between 230 and 290 K could be caused by unblocking of superparamagnetic magnetosomes and/or by the decrease in $|K_1|$ (Fischer *et al.* 2008). The plateau-like development of ΔB_{eff} between T_i and 230 K indicates that the diminishment of the interaction-induced shape anisotropy caused no marked change in the overall anisotropy. The FMR spectra reported by Fischer *et al.* (2008) show that this balance of overall anisotropy can be perturbed by exposing the sample in the cavity to a field (0.25 T) between the measurements, which induces a B_{uni}. Such an effect was also observed by electron holography where magnetic induction directions occurred along chain axes at low temperature close to T_V (Simpson *et al.* 2005).

3.4 Implication for the detection of magnetofossils

Magnetofossils are the mineral remains of MTB preserved in geological systems. As mentioned above, the cellular dipole in MTB is formed via the assembly of SSD stabilized by intracellular cytoskeletal protein filaments (Scheffel *et al.* 2006). In a geological time frame the breakdown of proteins because of diagenesis is relatively fast in sedimentary environments. This means that magnetofossils are generally preserved as chain fragments or loosely arranged SSD magnetite in non-turbulent environments, such as deep sea or lake sediments (e.g. Petersen *et al.* 1986; Paasche & Larson 2010). Moreover, it is very likely that the alignment of the magnetosomes and their easy axes associated with magnetofossils becomes perturbed during diagenesis. In such a case the contribution of the interaction-induced anisotropy to the total anisotropy of magnetofossils is diminished. Considering the low-temperature FMR analysis between room temperature and T_i, where the crystallographic structure of the magnetosomes is cubic, a similar decrease in the contribution of interaction-induced shape anisotropy is indicated by the increase of g_{eff} and the loss of well-resolved spectral features in the low-field range with temperature as well as the spectral simulations (Figs 3 and 5). Because the cellular dipoles of MTB upon cooling to T_i are critically affected by $|K_1|$ (Fischer *et al.* 2008), the diminishment of interaction-induced shape anisotropy

should be observed in MTB and magnetofossils independent from their magnetosome morphology.

The critical spectral hallmarks for the detection of MTB and their remains are g_{eff} values close to or less than two and an asymmetric line-shape with distinct features such as peaks or shoulders (e.g. Weiss *et al.* 2004). In fact, the few FMR spectra of magnetofossils published (e.g. Kopp *et al.* 2006) are quite similar to our spectra close to the isotropic point T_{i}. Therefore, the decrease of the interaction-induced shape anisotropy in intact MTB can be revealed by FMR spectroscopy. This can be used as guidance for the detection of magnetofossils in geological systems, in which diagenesis often reduces such anisotropy. Beyond that, such detection could make a valuable physical contribution to unravel the microbial evolution during Earth's history.

4 CONCLUSION

The continued low-temperature FMR spectral series provides an insight into anisotropy changes of magnetite in MTB at the T_{V} and into the interaction-induced shape anisotropy forming the cellular dipole. The diminishment in strength of this dipole is indicated by the vanishing of the two distinct low-field spectral features and the shift of g_{eff} to higher values between room temperature and the isotropic point T_{i} and further confirmed by the analytical derivation of the spectra. This weakening of uniaxiality in intact MTB with temperature is comparable to the effect that can be generated by the disintegration of magnetosome chains. Based on spectral analogies, low-temperature FMR spectra of intact MTB can be used a guidance to detect magnetofossils.

ACKNOWLEDGMENT

REFERENCES

Bazylinski, D.A. & Frankel, R.B., 2004. Magnetosome formation in prokaryotes, *Nat. Rev. Microbiol.,* **2,** 217–230.

Bickford, L.R., 1950. Ferromagnetic absorption in magnetite single crystals, *Phys. Rev.,* **78,** 449–457.

Charilaou, M., Winklhofer, M. & Gehring, A.U., 2011. Simulation of ferromagnetic resonance spectra of linear chains of magnetite nano-crystals, *J. Appl. Phys.,* **109,** doi:10.1063/1.3581103.

Devouard, B., Pósfai, M., Hua X, Bazylinski, D.A., Frankel, R.B. & Buseck, P.R., 1998. Magnetite from magnetotactic bacteria: size distributions and twinning, *Am. Mineral.,* **83,** 1387–1398.

Ding, Y., LI, J., Yang, J., Jiang, W., Tian, J. Li, Y, Pan, Y & Li, J., 2010. Deletion of the ftsZ-like gene results in the production of superparamagnetic magnetite magnetosomes in Magnetospirillum gryphiswaldense, *J. Bacteriol.,* **192,** 1097–1105.

Dunin-Borkowski, R.E., McCartney, M.R., Frankel, R.B., Bazylinski, D.A., Pósfai, M. & Buseck, P.R., 1998. Magnetic microstructure of magnetotactic bacteria by electron holography, *Science,* **282,** 1868–1870.

Egli, R., Chen, A.P., Winklhofer, M., Kodama, K.P. & Horng, C.S., 2010. Detection of noninteracting single domain particles using first-order reversal curve diagrams, *Geochem. Geophys. Geosyst.,* **11,** Q01Z11, doi:10.1029/2009GC002916.

Faivre, D., Fischer, A., Garcia-Rubio, I., Mastrogiacomo, G. & Gehring, A.U., 2010. The development of cellular magnetic dipoles in magnetotactic bacteria, *Biophys. J.,* **99,** 1266–1273.

Fischer, H., Mastrogiacomo, G., Löffler, J.F., Warthmann, R.J., Weidler, P.G. & Gehring, A.U., 2008. Ferromagnetic resonance and magnetic characteristics of intact magnetosome chains in *Magnetospirillum gryphiswaldense, Earth planet. Sci. Lett.,* **270,** 200–208.

Frankel, R.B., Blakemore, R.P. & Wolfe, R.S., 1979. Magnetite in freshwater magnetotactic bacteria, *Science,* **203,** 1355–1356.

Garcia, J. & Subias, G., 2004. The Verwey transition – a new perspective, *J. Phys. Condens. Matter,* **16,** R145–R178.

Gehring, A.U., Kind, J., Charilaou, M. & Garcia-Rubio, I., 2011. The detection of magnetotactic bacteria and magnetofossils by means of magnetic anisotropy, *Earth planet. Sci. Lett.,* **309,** doi:10.1016/j.epsl.2011.06.024.

Hanzlik, M., Winklhofer, M. & Petersen, N., 2002. Pulsed-field-remanence measurements on individual magnetotactic bacteria, *J. Magn. Magn. Mater.,* **248,** 258–267.

Heider, F. & Williams, W., 1988. Note on the temperature dependence of exchange constant in magnetite, *Geophys. Res. Lett.,* **15,** 184–187.

Heyen, U. & Schüler, D., 2003. Growth and magnetosome formation by microaerophilic Magnetospirillum strains in a oxygen-controlled fermentor. *Appl. Microbiol. Biotechnol.,* **61,** 536–544.

Jacobs, I.S. & Bean, C.P., 1955. An approach to elongated fine-particle magnets, *Phys. Rev.,* **100,** 1060–1067.

Kakol, Z. & Honig, J.M., 1989. Influence of deviations from the ideal stoichiometry on the anisotropy parameters of magnetite $Fe_3(1-\delta)O_4$, *Phys. Rev.,* **B 40,** 9090–9096.

Kopp, R.E. & Kirschvink, J.L., 2008. The identification and biochemical interpretation of fossil magnetotactic bacteria, *Earth-Sci. Rev.,* **86,** 42–61.

Kopp, R.E., Nash, C.Z., Kobayashi, A., Weiss, B.P, Bazylinski, D.A. & Kirschvink, J.L., 2006. Ferromagnetic resonance spectroscopy for assessment of magnetic anisotropy and magnetostatic interactions: a case study of mutant magnetotactic bacteria, *J. geophys. Res.,* **111,** B12S25, doi:10.1029/2006JB004529.

Kronmüller, H. & Walz, F., 1980. Magnetic after effects in Fe_3O_4 and vacancy-doped magnetite, *Philos. Mag.,* **B 42,** 433–452.

Li, J, Pan, Y., Chen, G., Liu, Q., Tian, L. & Lin, W., 2009. Magnetite magnetosome and fragmental chain formation of *Magnetospirillum magneticum* ABM-1: transmission electron microscopy and magnetic observations, *Geophys. J. Int.,* **177,** 33–42.

Mann, S., Frankel, R.B. & Blakemore, R.P., 1984. Structure, morphology, and crystal growth of bacterial magnetite, *Nature,* **310,** 405–407.

Mann, S., Sparks, N.H.C. & Blakemore, R.P., 1987. Ultrastructure and characterization of anisotropic magnetite inclusions in magnetotactic bacteria, *Proc. R. Soc. Lond.,* **B 231,** 469–476.

Mastrogiacomo, G., Fischer, H., García-Rubio, I. & Gehring, A.U., 2010. Ferromagnetic resonance spectroscopic response of magnetite chains in a biological matrix, *J. Magn. Magn. Mater.,* **332,** 661–663.

Moskowitz, B.M., Frankel, R.B. & Bazylinski, D.A., 1993. Rock magnetic criteria for the detection of biogenic magnetite, *Earth planet. Sci. Lett.,* **120,** 283–300.

Muxworthy, A.R. & McClelland, E., 2000. Review of the low-temperature magnetic properties of magnetite from a rock magnetic perspective, *Geophys. J. Int.,* **140,** 101–114.

Muxworthy, A.R. & Williams, W., 2006. Low temperature cooling behavior of single-domain magnetite: forcing of crystallographic axes and interactions, *J. geophys. Res.,* **111,** B07103, doi:10.1029/2006JB004298.

Özdemir, Ö., Dunlop, D. & Moskowitz, B.M., 2002. Changes in remanence, coercivity and domain state at low temperature in magnetite, *Earth planet. Sci. Lett.,* **194,** 343–358.

Paasche, Ø. & Larsen, J., 2010. Changes in lake stratification and oxygen distribution inferred from two contrasting records of magnetotactic bacteria and diatoms. *J. geophys. Res.,* **115,** G02012, doi:10.1029/2009JG001081.

Pan, Y., Petersen, N., Winklhofer, M., Davila, A.F., Li, Q., Frederichs, T., Hanzlik, M. & Zhu, R., 2005. Rock magnetic properties of uncultured magnetotactic bacrteria, *Earth planet. Sci. Lett.,* **237,** 311–325.

Penninga, I, de Waard, H., Moskowitz, B.M., Bazylinski, D.A. & Frankel, R.B., 1995. Remanence measurements on individual magnetotactic bacteria using a magnetic pulse field, *J. Magn. Magn. Mater.,* **149,** 275–286.

Petersen, N., Von Dobeneck, T. & Vali, H., 1986. Fossil bacterial magnetite in deep-sea sediments from the South Atlantic Sea, *Nature,* **320,** 611–615.

Pósfai, M., Moskowitz, B.M., Arató. B., Schüler, D., Flies, C., Bazylinski, D.A. & Frankel, R.B., 2006. Properties of intracellular magnetite crystals produced by *Desulfovibro magneticus* strain RS-1, *Earth planet. Sci. Lett.,* **249,** 444–455.

Prozorov, R., Prozorov, T., Mallapragada, S.K., Narasimhan, B., Williams, T.J. & Bazylinski, D.A., 2007. Magnetic irreversibility and the Verwey transition in nanocrytsalline bacterial magnetite, *Phys. Rev.,* **B 76,** 054406-1–054406-9.

Scheffel, A., Gruska, M., Faivre, D., Linaroudis, A., Plitzko, J.M & Schüler, D., 2006. An acidic protein aligns magnetosomes along a filamentous structure in magnetotactic bacteria, *Nature,* **440,** 110.

Simmons, S.L., Bazylinski, D.A. & Edwards, K.J., 2006. South-seeking magnetotactic bacteria in the Northern Hemisphere, *Science,* **311,** 371–374.

Simpson, E.T., Kasama, T., Pósfai, M., Buseck, P.R., Harrison, R.J. & Dunin-Borkowski, R.E., 2005. Magnetic induction mapping of magnetite chains in magnetotactic bacteria at room temperature and close to the Verwey transition, *J. Phys. Conf. Ser.,* **17,** 108–121.

Snowball, I., 1994. Bacterial magnetite and magnetic properties of sediments in a Swedish lake, *Earth planet. Sci. Lett.,* **126,** 129–142.

Verwey, E.J.W., 1939. Electronic conduction of magnetite (Fe_3O_4) and its transition point at low temperatures, *Nature,* **144,** 327–328.

Walz, F., 2002. The Verwey transition – a topical review, *J. Phys. Condens. Matter,* **14,** R285–R340.

Weiss, B.P., Kim, S.S., Kirschvink, J.L., Kopp, R.E., Sankaran, M., Kobayashi, A. & Komeili, A., 2004. Ferromagnetic resonance and low-temperature magnetic tests for biogenic magnetite, *Earth planet. Sci. Lett.,* **224,** 73–89.

Wright, J.P, Attfield, J.P. & Radaelli, P.G., 2002. Charge ordered structure of magnetite Fe_3O_4 below the Verwey transition, *Phys. Rev.,* **B 66,** 214422.